Josephson effect in superconductor/ferromagnet structures with a complex weak-link region

T. Yu. Karminskaya,[1] A. A. Golubov,[2] M. Yu. Kupriyanov,[1] and A. S. Sidorenko[3,4]
[1]*Nuclear Physics Institute, Moscow State University, 119992 Moscow, Russia*
[2]*Faculty of Science and Technology and MESA+ Institute of Nanotechnology, University of Twente, P.O. Box 217, 7500 AE Enschede, The Netherlands*
[3]*Institute of Nanotechnology, Karlsruhe Institute of Technology, D-76021 Karlsruhe, Germany*
[4]*Institute of Electronic Engineering and Industrial Technologies, Chisinau, Moldova*
(Received 6 April 2010; published 18 June 2010)

The critical currents I_C of SNF-FN-FNS, SN-FN-NS, and SNF-N-FNS Josephson junctions (S—superconductor, F—ferromagnetic, N—normal metal) with complex SNF or SN electrodes (N or NF bilayer are situated under a superconductor) are calculated in the framework of linearized Usadel equations for arbitrary overlap length d of SN interface. We demonstrate that in these geometries, in the case of large resistances of SN interfaces, the critical current can exceed that in ramp-type junctions. Based on these results, the choice of the most practically applicable geometry is discussed. We predict that in a certain parameter range there is single 0-π transition with the increase in the overlap length d. This single transition can be realized also in SFN-N-FNS Josephson junctions, where the coherence length in the weak-link region is a real quantity. Further, we predict that in SNF-N-FNS Josephson junctions 0-π transition may take place with increase in distance between superconducting electrodes.

DOI: 10.1103/PhysRevB.81.214518 PACS number(s): 74.45.+c

I. INTRODUCTION

In the last few years there is a significant interest to the structures composed from ferromagnetic (F) and superconducting (S) layers.[1–3] This interest is permanently maintained due to possible application of SF structures in quantum computing and superconducting electronics,[4–8] as well as due to new fundamental physical effects, which are steadily observed experimentally (see, e.g., Refs. 9–16) or predicted theoretically (see, e.g., Refs. 17–54).

Among the most appealing recent experimental results are: the first observation of double suppression of superconductivity in Nb/Cu_xNi_{1-x} bilayers ($x=0.59$), which provides evidence for a multiple re-entrant superconducting state;[11] the demonstration of existence of a long-range proximity effect predicted in Ref. 3 in Nb-Cu/PdNi/Cu/CoReCo/Cu/PdNi/Cu-Nb Josephson junctions, where the direction of magnetization vector in antiferromagnetically oriented CoReCo block does not coincide with that of PdNi films, thus creating a weak-link region with artificially rotated magnetization vector;[12] the first observation[13] of strong critical temperature suppression in S-FNF (N—normal metal) structures under a small off-orientation of magnetization vectors in initially antiferromagnetically ordered FNF block, which is a sequent of generation of long-range triplet component providing a strong connection of NF part of the multilayer to the S film;[55] visualization of supercurrent spatial distribution in SFS devices with various arrangements of 0 and π segments.[16]

Despite of noticeable achievement in understanding of the physical background of superconducting spin valves, in which either critical temperature T_C or critical current I_C is controlled by mutual off-orientation of magnetization vectors $\mathbf{M}_{1,2}$ of individual F films located inside of a spin valve, they are still far from practical realization. Among the reasons are relatively large values of exchange energies H in F films resulting in very fast decay of superconducting correlations into a ferromagnet,[56,57] as well as the problems in supply of off-orientation of $\mathbf{M}_{1,2}$ in Josephson spin valves.

Recently[50–53] it has been shown that both problems can be effectively solved in novel types of S-FN-S and S-FNF-S Josephson junctions. In these structures, the weak-link region consists of FN or FNF multilayer, which separates the superconducting banks while a supercurrent flows in the direction parallel to FN interfaces and is injected across the end walls of FN or FNF structure. There are two kinds of proximity effects in these junctions. The first one is the penetration of superconductivity into normal metal from superconducting electrodes. The second one is the suppression of the induced superconductivity due to interaction between N and F layers. It is obvious that for nontransparent NF interfaces the S-FNF-S junction should have the same characteristics as that of SNS devices and the decay length of superconducting correlations into the complex weak-link region should coincide with that for the normal metal, ξ_N, if the distance between superconducting electrodes L are larger than the scale ξ_{F1} of superconductivity decay into F films. In Refs. 50–53, it was also shown that switching on interaction between N and F metals results in generation of a set of decay lengths. Moreover, it was demonstrated that it is possible to find the conditions under which at least one among these lengths has both real and imaginary parts on the order of ξ_N. In S-FNF-S Josephson devices, there is no limitation on thickness of N film and it can be made thin enough to realize an effective control upon the junction parameters by changing the mutual orientation of magnetization vectors of ferromagnetic films.[52]

The choice of junction geometry considered in Refs. 50–53 was based on existing concept[58,59] that in such ramp-type configuration both the critical current I_C and I_CR_N product (R_N is the normal junction resistance) are larger than in overlap geometry when S electrodes are located on the top of weak-link multilayer.

 ©2010 The American Physical Society

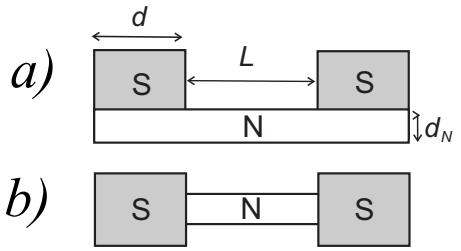

FIG. 1. (a) The SN–N–NS junction and (b) the SNS junction.

In this paper, we reconsider this statement and demonstrate that it is valid only for the fully transparent interfaces between S electrodes and a weak-link region. To do this we study three different geometries of Josephson junctions: (1) SN-NF-NS devices, which consist of two SN complex electrodes connected by NF weak region; (2) SNF-N-FNS structures in which N film connects two SNF complex electrodes, and (3) SNF-NF-FNS junctions with S electrodes located on the top of FN bilayer. Below we will discuss critical currents of these Josephson structures in the framework of linearized Usadel equations for arbitrary length of complex electrodes. We will compare the results for the above three cases and those obtained in Refs. 50–53 in order to determine the geometry, which provides the largest magnitude of the critical current. We also demonstrate that 0-π transition in the considered structures can be driven not only by variation in distance L between S electrodes, as predicted by known models, but also by changing the length d of the SNF overlap region.

II. MODEL

Consider multilayered structures presented in Figs. 1 and 2. They consist of superconducting electrodes with the length d deposited on the top either a single N film or on NF bilayer. The bilayer consists of F and N films having a thickness d_F and d_N, respectively (see Fig. 2). The junctions shown in Figs. 1(b) and 2(d) are the structures having ramp-type geometry intensively studied previously (see Refs. 1–3, 50–53, and 58). The width of layers in the direction perpendicular to the current flow is equal to W and the distance between electrodes is L. We will suppose that the condition of a dirty limit is fulfilled for all metals and that effective electron-phonon coupling constant is zero in F and N materials. For simplicity, we suggest below that the parameters γ_{BN} and γ_{BF} which characterize the transparency of NS and FS interfaces,

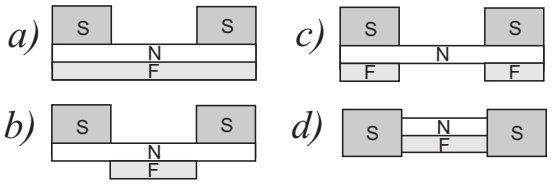

FIG. 2. (a) The SNF–NF–FNS junction, (b) the SN–NF–NS junction, (c) the SNF–N–FNS junction, and (d) the S–NF–S junction.

$$\gamma_{BN} = R_{BN}\mathcal{A}_{BN}/\rho_N\xi_N, \quad \gamma_{BF} = R_{BF}\mathcal{A}_{BF}/\rho_F\xi_F$$

are large enough

$$\gamma_{BN} \gg \max\left\{1, \frac{\rho_S\xi_S}{\rho_N\xi_N}\right\}, \quad \gamma_{BF} \gg \max\left\{1, \frac{\rho_S\xi_S}{\rho_F\xi_F}\right\}, \qquad (1)$$

to neglect the suppression of superconductivity in S part of the proximity system. Here R_{BN}, R_{BF} and $\mathcal{A}_{BN}$, $\mathcal{A}_{BF}$ are the resistances and areas of the SN and SF interfaces, ξ_S, ξ_N, and ξ_F are the decay lengths of S, N, and F materials while ρ_S, ρ_N, and ρ_F are their resistivities.

We assume that either temperature T is close to the critical temperature of superconducting electrodes T_C or parameters γ_{BN} and γ_{BF} are large enough to permit the use of the linearized Usadel equations in F and N films of the structure. Under the above conditions the problem of calculation of the critical current in the structures reduces to solution of the set of linearized Usadel equations for anomalous Green's functions $\Phi_{N,F}$,[1–3,60]

$$\xi_N^2\left\{\frac{\partial^2}{\partial x^2} + \frac{\partial^2}{\partial y^2}\right\}\Phi_N - \Omega\Phi_N = 0,$$

$$\xi_F^2\left\{\frac{\partial^2}{\partial x^2} + \frac{\partial^2}{\partial y^2}\right\}\Phi_F - \tilde{\Omega}\Phi_F = 0, \qquad (2)$$

where $\Omega = |\omega|/\pi T_C$, $\tilde{\Omega} = [|\omega| + iH\,\mathrm{sgn}(\omega)]/\pi T_C$, $\xi_{N,F}^2 = (D_{N,F}/2\pi T_C)$, $D_{N,F}$ are diffusion coefficients, $\omega = \pi T(2n+1)$ are Matsubara frequencies, and H is exchange integral of ferromagnetic material. To write Eq. (2) we have chosen the x and y axes in the directions perpendicular and parallel to the plane of N film and put the origin in the middle of structure at FN interface [Figs. 2(a), 2(b), and 2(d)] or at the lower free interface of N film [Figs. 1 and 2(c)].

Equations (2) must be supplemented by the boundary conditions.[61] For the structures presented in Figs. 1(b) and 2(d) they have the form

$$\gamma_{BN}\xi_N\frac{\partial}{\partial y}\Phi_N = \pm G_0\Delta\,\exp\left\{\pm i\frac{\varphi}{2}\right\}, \quad y = \pm L/2,$$

$$\gamma_{BF}\xi_F\frac{\partial}{\partial y}\Phi_F = \pm G_0\Delta\,\exp\left\{\pm i\frac{\varphi}{2}\right\}, \quad y = \pm L/2 \qquad (3)$$

while for the junctions presented in Figs. 1(a) and 2(a)–2(c) they can be written as

$$\gamma_{BN}\xi_N\frac{\partial}{\partial x}\Phi_N = G_0\Delta\,\exp\left\{\pm i\frac{\varphi}{2}\right\}, \quad x = d_N, \qquad (4)$$

where Δ and φ are the modulus and the phase difference of the order parameters of superconducting electrodes.

At SF interfaces [see Fig. 2(d)] we also have

$$\gamma_{BF}\xi_F\frac{\partial}{\partial y}\Phi_F = \pm\frac{\tilde{\Omega}}{\Omega}G_0\Delta\,\exp\left\{\pm i\frac{\varphi}{2}\right\}, \quad y = \pm L/2. \qquad (5)$$

Here L is the distance between superconducting electrodes, $G_0 = \omega/\sqrt{\omega^2+\Delta^2}$.

At the FN interface located at $(x=0)$ the boundary conditions have the form[61]

$$\frac{\xi_N}{\Omega}\frac{\partial}{\partial x}\Phi_N = \gamma\frac{\xi_F}{\tilde{\Omega}}\frac{\partial}{\partial x}\Phi_F, \tag{6}$$

$$\gamma_B\xi_F\frac{\partial}{\partial x}\Phi_F + \Phi_F = \frac{\tilde{\Omega}}{\Omega}\Phi_N, \tag{7}$$

where $\gamma_B = R_{B3}\mathcal{A}_{B3}/\rho_F\xi_F$, $\gamma = \rho_N\xi_N/\rho_F\xi_F$, R_{B3} and $\mathcal{A}_{B3}$ are the resistance and area of the NF interface.

The boundary conditions at free interfaces come from the demand of an absence of a current across them and reduce to equality to zero of appropriate derivatives, e.g., for the junction presented in Fig. 2(d) they look as

$$\frac{\partial}{\partial x}\Phi_N = 0, \quad x = d_N, \tag{8}$$

$$\frac{\partial}{\partial x}\Phi_F = 0, \quad x = -d_F. \tag{9}$$

The formulated above boundary problems can be reduced from two-dimensional to one-dimensional models in the limit of small thicknesses of N and F films

$$d_N \ll \xi_N, \quad d_F \ll \xi_F. \tag{10}$$

This procedure has been described in detail in Refs. 50–52 and the range of its validity has been examined in Ref. 53. Below we will apply the developed in[50–52] approach to the junctions presented in Figs. 1 and 2 mostly being concentrated on the discussion of the obtained results. The details of calculations are summarized in Appendices A and C.

III. CRITICAL CURRENT OF SN-N-NS JOSEPHSON JUNCTION

The expressions for the critical currents, I_C^{SNS}, $I_C^{\mathrm{SN\text{-}N\text{-}NS}}$, of SNS junction shown in Fig. 1 are well known in the considered model.[1,62] They have the form

$$I_C^{\mathrm{SNS}} = K\frac{d_N}{\xi_N}\sum_{n=0}^{\infty}\frac{\Gamma}{q\,\sinh(qL)}, \tag{11}$$

$$I_C^{\mathrm{SN\text{-}N\text{-}NS}} = \frac{K}{\xi_N d_N}\sum_{n=0}^{\infty}\frac{\Gamma\,\sinh^2(qd)}{q^3\,\sinh[q(L+2d)]}, \tag{12}$$

where coefficient $K=(2\pi TW)/(R_{BN}\mathcal{A}_{BN}\gamma_{BN}e)$, $q=\xi_N^{-1}\sqrt{\Omega}$ is inverse decay length, and $\Gamma=\Delta^2/(\omega^2+\Delta^2)$.

As it is shown in Appendices A and C, the expression (12) also follows from more general formula for the critical current of SNF-NF-SNF devices shown in Fig. 2(a) in the limit of small thickness of F film $(d_F\to 0)$. The ratio of these two critical currents, $I_C^{\mathrm{SN\text{-}N\text{-}NS}}/I_C^{\mathrm{SNS}}$, is visualized in Fig. 3 as a function of thickness of normal layer, d_N, for several lengths of complex electrode $d/\xi_N=0.5,1,10$. It is clearly seen that there are intervals of parameters under which critical current of SN-N-NS junction can essentially exceed I_C^{SNS}. The physics of this effect is evident as we are going to discuss now.

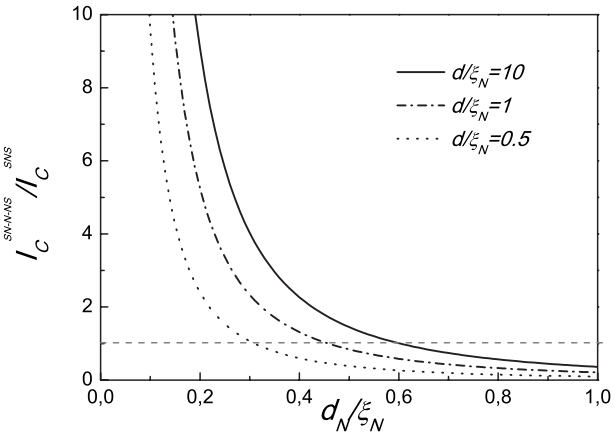

FIG. 3. $I_C^{\mathrm{SN\text{-}N\text{-}NS}}/I_C^{\mathrm{SNS}}$ versus thickness of N film d_N/ξ_N for $d/\xi_N=0.5,1,10$, $L/\xi_N=2$, and $T/T_C=0.5$.

In the considered limit of small SN interface transparency for ramp-type geometry [Fig. 1(b)] under condition $L\gg 1/q$ the magnitude of induced into N metal Φ_N functions at SN interfaces is close to

$$\Phi_N(d_N) = \frac{G_0\Delta}{\gamma_{BN}\xi_N q}, \quad \gamma_{BN}\xi_N q \gg 1 \tag{13}$$

while in the case of the overlap geometry [Fig. 1(a)] for $d_N \ll 1/q$ the magnitude of Φ_N function in N metal does not depend on the coordinate x in the first approximation in d_N/ξ_N and is equal to

$$\Phi_N(d_N) = \frac{G_0\Delta}{\gamma_{BN}\xi_N q^2 d_N}, \quad \gamma_{BN}\xi_N q^2 d_N \gg 1. \tag{14}$$

From Eqs. (13) and (14) it immediately follows that the large factor γ_{BN} in Eq. (14) can be renormalized by a small ratio of d_N/ξ_N thus leading to effective increase in superconductivity at the interface between N film and SN composite electrode compared to the strength of superconducting correlations at SN boundary of SNS ramp-type devices.

IV. CRITICAL CURRENT OF DEVICES WITH F FILM IN WEAK-LINK REGION

To calculate the critical current of the junctions shown in Fig. 2 under conditions (1) and (10) one has to solve the boundary problem, Eqs. (2)–(8), and substitute the obtained solution into general formula for supercurrent,

$$I_S = \frac{-i\pi TW}{e\rho_F}\sum_{\omega=-\infty}^{\infty}\frac{1}{\tilde{\omega}^2}\int_{-d_F}^{0}\left[\Phi_{-\omega,F}^{*}\frac{\partial}{\partial y}\Phi_{\omega,F}\right] - \frac{i\pi TW}{e\rho_N}\sum_{\omega=-\infty}^{\infty}\frac{1}{\omega^2}\int_{0}^{d_N}\left[\Phi_{-\omega,N}^{*}\frac{\partial}{\partial y}\Phi_{\omega,N}\right]. \tag{15}$$

The details of this procedure are given in Appendices A and C.

It is shown there that in the practically interesting limit of strong N film,

$$\zeta_N \gg \zeta_F, \quad \xi_N \gg \xi_F, \tag{16}$$

where parameters ζ_F and ζ_N are the coupling constants $\zeta_F^2 = \gamma_B d_F \xi_F$, $\zeta_N^2 = \gamma_B d_N \xi_N / \gamma$, which describe the mutual influence of N and F films on superconducting correlations in the junction, the critical current of SNF-NF-FNS [Fig. 2(a)], SN-NF-NS [Fig. 2(b)], and SNF-N-FNS [Fig. 2(c)] structures,

$$I_C^{\text{SNF-NF-FNS}} = \frac{K}{\xi_N d_N} \text{Re} \sum_{n=0}^{\infty} \frac{\Gamma U q_1 \sinh^2(q_1 d)}{\sinh[q_1(L+2d)]}, \tag{17}$$

$$I_C^{\text{SN-NF-NS}} = \frac{K}{\xi_N d_N} \text{Re} \sum_{n=0}^{\infty} \frac{\Gamma q_1}{q^4 (Q_{q,q_1} + P_{q,q_1})}, \tag{18}$$

$$I_C^{\text{SNF-N-FNS}} = \frac{K}{\xi_N d_N} \text{Re} \sum_{n=0}^{\infty} \frac{\Gamma U q}{Q_{q_1,q} + P_{q_1,q}} \tag{19}$$

can be expressed by formulas (17)–(19), respectively. Here, functions $Q(\alpha,\beta)$, $P(\alpha,\beta)$, and U are defined as

$$Q_{a,b} = \frac{2 \coth(ad) \cosh(bL) b}{a}, \tag{20}$$

$$P_{a,b} = \sinh(bL) \left[1 + \frac{b^2 \coth^2(ad)}{a^2} \right], \tag{21}$$

$$U = \left(\frac{v^2 \zeta_F^2 \zeta_N^2}{1 - v^2 u^2 \zeta_F^2 \zeta_N^2} \right)^2, \tag{22}$$

where q_1 is fundamental wave vector of the problem,

$$q_1^2 = \frac{1}{2} [u^2 + v^2 - \sqrt{(u^2 - v^2)^2 + 4 \zeta_F^{-2} \zeta_N^{-2}}] \tag{23}$$

while u and v,

$$u^2 = \left(\frac{1}{\zeta_N^2} + \frac{\Omega}{\xi_N^2} \right), \quad v^2 = \left(\frac{1}{\zeta_F^2} + \frac{\Omega}{\xi_F^2} + i \frac{h}{\xi_F^2} \right), \tag{24}$$

are partial wave vectors. Strictly speaking, formulas (17)–(19) are valid in the limit of thin N and F films, Eq. (10). However, making use of the formalism developed in Ref. 53 it is possible to prove that all of them can also be valid for arbitrary thickness of F film if one simply use in Eqs. (17)–(19) the more general expression for fundamental wave vector q_1, namely,

$$q_1 = \frac{1}{\xi_N} \sqrt{\frac{\xi_N}{d_N} \frac{\gamma \sqrt{\tilde{\Omega}}}{\gamma_B \sqrt{\tilde{\Omega}} + \coth\left\{ \frac{d_F}{\xi_F} \sqrt{\tilde{\Omega}} \right\}}} + \Omega. \tag{25}$$

Expressions (17)–(19) can be simplified in several practically interesting cases.

In the limit of large $d (d \gg 1/q, 1/q_1)$, both $\coth(qd) \to 1$ and $\coth(q_1 d) \to 1$. As a result for SN-NF-NS and SNF-N-NFS junctions one may use the same formulas (18) and (19) with more simple forms of functions $Q(\alpha,\beta)$ and $P(\alpha,\beta)$,

$$Q_{a,b} = \frac{2 \cosh(bL) b}{a}, \tag{26}$$

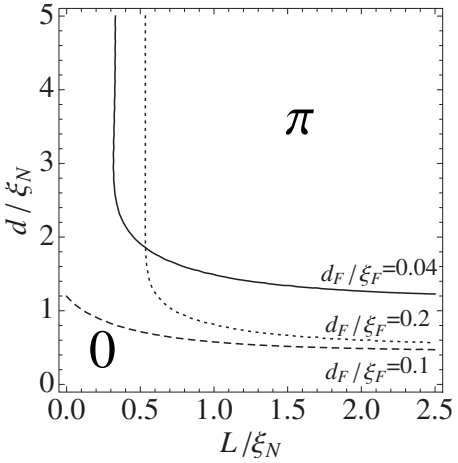

FIG. 4. $(L/\xi_N, d/\xi_N)$ phase diagram for SNF-N-FNS structure for $d_F/\xi_F = 0.04, 0.1, 0.2$ (solid, dashed, and dotted lines) at $\gamma = 0.1$, $\gamma_B = 0.1$, $d_N/\xi_N = 0.1$, $\xi_N/\xi_F = 10$, $T/T_C = 0.5$, and $H/\pi T_C = 30$.

$$P_{a,b} = \sinh(bL) \left(1 + \frac{b^2}{a^2} \right) \tag{27}$$

while for SNF-NF-FNS junction

$$I_C^{\text{SNF-NF-FNS}} = \frac{1}{2} \frac{K}{\xi_N d_N} \text{Re} \sum_{n=0}^{\infty} \Gamma U q_1 \exp(-q_1 L). \tag{28}$$

In the limit of large distance L between S electrodes, $L \gg 1/q$, $1/q_1$ for the critical current of SNF-NF-FNS, SN-NF-NS, and SNF-N-NFS one can get, respectively,

$$I_C^{\text{SNF-NF-FNS}} = \frac{2K}{\xi_N d_N} \text{Re} \sum_{n=0}^{\infty} \frac{\Gamma U q_1 \exp(-q_1 L)}{[1 + \coth(qd)]^2} \tag{29}$$

$$I_C^{\text{SN-NF-NS}} = \frac{2K}{\xi_N d_N} \text{Re} \sum_{n=0}^{\infty} \frac{\Gamma q_1 \exp(-q_1 L)}{q^2 [q + q_1 \coth(qd)]^2}, \tag{30}$$

$$I_C^{\text{SNF-N-FNS}} = \frac{2K}{\xi_N d_N} \text{Re} \sum_{n=0}^{\infty} \frac{\Gamma U q q_1^2 \exp(-qL)}{[q_1 + q \coth(q_1 d)]^2}. \tag{31}$$

Below we will compare the obtained results (17)–(19) with the value of the critical current calculated in Ref. 50 for ramp-type SFNS junction,

$$I_C^{\text{SFNS}} = K \frac{d_N}{\xi_N} \text{Re} \sum_{n=0}^{\infty} \Gamma \frac{\left(1 - \frac{1}{q_1^2 - v^2} \frac{\gamma_{BN}}{\gamma_{BF}} \frac{\xi_N}{\xi_F \zeta_N^2} \right)^2}{q_1 \sinh(q_1 L)}. \tag{32}$$

It is necessary to mention that in the limit of decoupled F and N films $(\gamma_B \to \infty)$ expressions for the critical currents [Eqs. (17)–(19)] reduce to the formula for SN-N-NS devices, Eq. (12), while the critical current of SFNS ramp-type structure, Eq. (32), transforms to that, Eq. (11), valid for SNS junctions.

Below we will restrict ourselves by analysis of $I_C(L,d)$ dependencies. In Figs. 4–9 we present the phase diagrams for critical current, which in $(L/\xi_N, d/\xi_N)$ plane gives the

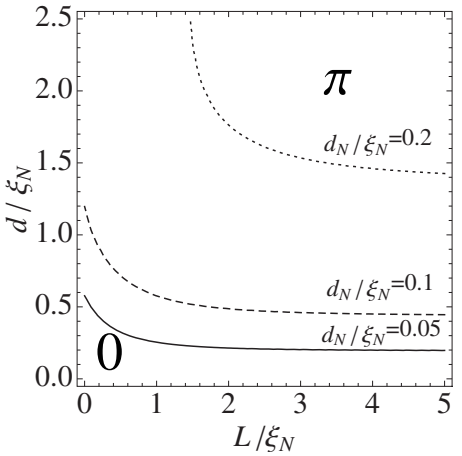

FIG. 5. $(L/\xi_N, d/\xi_N)$ phase diagram for SNF-N-FNS structure for d_N/ξ_N=0.05,0.1,0.2 (solid, dashed, and dotted lines) at γ=0.1, γ_B=0.1, d_F/ξ_F=0.1, ξ_N/ξ_F=10, T/T_C=0.5, and $H/\pi T_C$=30.

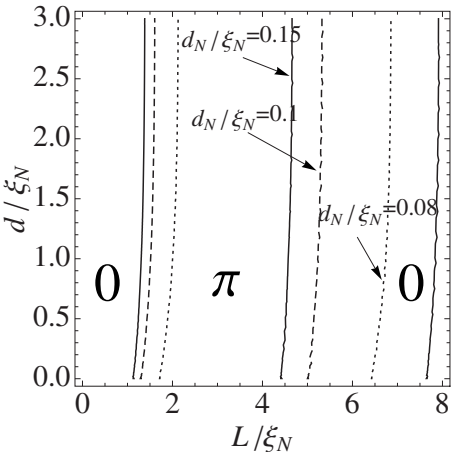

FIG. 7. $(L/\xi_N, d/\xi_N)$ phase diagram for SN-FN-NS structure for d_N/ξ_N=0.08,0.1,0.15 (solid, dashed, and dotted lines) at γ=0.1, γ_B=0.1, d_F/ξ_F=0.1, ξ_N/ξ_F=10, T/T_C=0.5, and $H/\pi T_C$=30.

information about the sign of I_C. In the areas marked in Figs. 4–9 by 0 and π the critical current is positive (0 state) and negative (π state), correspondingly, while the lines give the point curves at which I_C=0. The position of these curves in $(L/\xi_N, d/\xi_N)$ plane also depends on relative thickness (d_F/ξ_F and d_N/ξ_N) of both F and N films.

The phase diagrams for SNF-N-FNS structures are given in Figs. 4 and 5. In this geometry there is the only N film in the region between SNF multilayers. The inverse coherence length $q=\xi_N^{-1}\sqrt{\Omega}$ in N film is real, therefore there are no oscillations of critical current in the structure.

Our calculations show that in this case there can be only one curve on the $(L/\xi_N, d/\xi_N)$ plane, at which I_C=0 for fixed other parameters. The existence of only one point curve for SNF-N-FNS structure can be understood from the following arguments. Contrary to the well-studied SFS junctions, the coherence length in the part of weak-link region of SNF-N-FNS devices located between SNF electrodes is real, thus preventing the oscillations of function Φ_N in that region of the N film. The oscillations of the condensate function exist only in the NF part of the weak link located under the S electrodes. Obviously, under these circumstances the sign of I_C must be only controlled by the value of the condensate function at the boundary between the SNF electrodes and the N film connecting the electrodes. As shown in Appendix B, this value of condensate function determines two complex coefficients, A_1 and A_2, [see Eqs. (B6) and (B7)]. In combination with nonoscillatory decay of function Φ_N into the N film from the SNF electrodes, these coefficients provide only two choices for the sign of I_C and only one curve at which I_C=0. This is in contrast to SFS devices with F film in between S electrodes. In the latter case the sign of I_C depends also on relation between the geometrical size of a junction and the imaginary part of the coherence length (the period of oscillations of the order parameter). It is the combination of these two factors that provides the opportunity to have multiple changes in I_C sign and infinite number of curves at $(L/\xi_N, d/\xi_N)$ plane at which I_C=0.

Therefore, in the considered SNF-N-FNS structures there is only one of these two factors and only one opportunity for I_C to change its sign, which can be realized or not depending

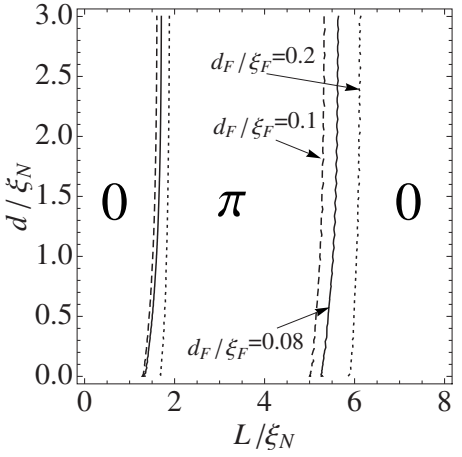

FIG. 6. $(L/\xi_N, d/\xi_N)$ phase diagram for SN-FN-NS structure for d_F/ξ_F=0.08,0.1,0.2 (solid, dashed, and dotted lines) at γ=0.1, γ_B=0.1, d_N/ξ_N=0.1, ξ_N/ξ_F=10, T/T_C=0.5, and $H/\pi T_C$=30.

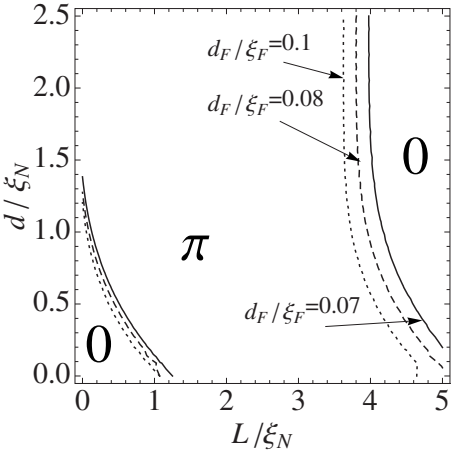

FIG. 8. $(L/\xi_N, d/\xi_N)$ phase diagram for SNF-FN-FNS structure for d_F/ξ_F=0.07,0.08,0.1 (solid, dashed, and dotted lines) at γ=0.1, γ_B=0.1, d_N/ξ_N=0.1, ξ_N/ξ_F=10, T/T_C=0.5, and $H/\pi T_C$=30.

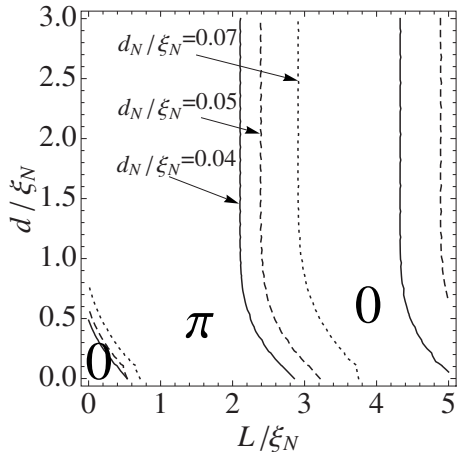

FIG. 9. $(L/\xi_N, d/\xi_N)$ phase diagram for SNF-FN-FNS structure for d_N/ξ_N=0.04,0.05,0.07 (solid, dashed, and dotted lines) at γ =0.1, γ_B=0.1, d_F/ξ_F=0.1, ξ_N/ξ_F=10, T/T_C=0.5, and $H/\pi T_C$=30.

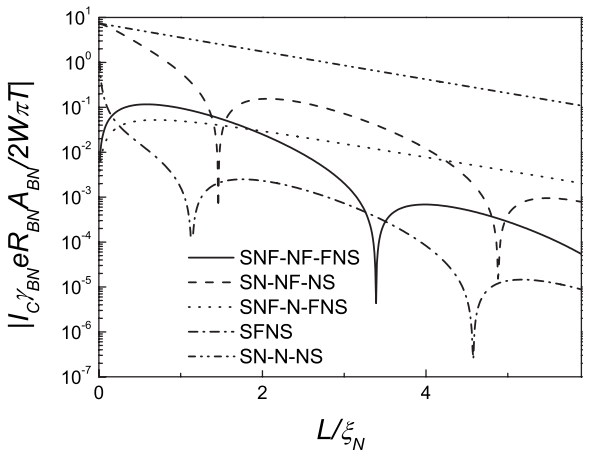

FIG. 10. I_C for SN-N-NS, SFNS, SNF-N-FNS, SN-FN-NS, SNF-FN-FNS structures versus L/ξ_N calculated for ξ_N/ξ_F=10, T/T_C=0.5, $H/\pi T_C$=30, d_N/ξ_N=0.1, and d_F/ξ_F=0.1.

on the parameters of the structure. The position of the transition curve calculated for fixed ratio d_N/ξ_N=0.1 and several values of d_F/ξ_F=0.04,0.1,0.2 is shown in Fig. 4. The location of the curve depends on d_F by nonmonotonic way. At d_F=0 there is only 0 state in the structure. With the increase in d_F, the curve first shifts to the left bottom corner of the phase diagram, then it turns back, and at some critical value of d_F it tends to infinity, thus providing only 0 state in the structure with further d_F increase. Such nonmonotonic behavior is due to nonmonotonic behavior of q_1 from Eq. (25).

Figure 5 shows $(L/\xi_N, d/\xi_N)$ phase diagram calculated for fixed ratio d_F/ξ_F=0.1 and several values of d_N/ξ_N =0.05,0.1,0.2. It is seen that with d_N increase the point curves at which I_C=0 shifts in the direction to the right corner of diagram providing the increase in area for 0 state. This fact can be understood if one takes into account that under fixed d_F the larger is the N layer thickness, the smaller is the influence of the F layer on the junction properties. It is obvious that at $d_N \gtrsim \xi_N$ the critical current of SNF-N-FNS junction will tend to that of SN-N-NS since the current will flow in the areas located closer to S electrodes thus decreasing the probability to have SNF-N-FNS structure in the π state. Also it is important to mention that at some fixed parameters only 0 state or π state can be realized for any L and at some fixed parameters only 0 state can be realized for any d.

The phase diagrams for SN-FN-NS structures are given in Figs. 6 and 7. Figure 6 presents the data calculated under fixed value of d_N/ξ_N=0.1 for a set of ratio d_F/ξ_F =0.08,0.1,0.2 while Fig. 7 gives diagram obtained under fixed value of d_F/ξ_F=0.1 for a set of parameters d_N/ξ_N =0.08,0.1,0.15. In this geometry there is the only N film in the complex SN electrodes. The inverse coherence length q in N film is real value. Consequently, both 0 and π states in SN-FN-NS junctions can be realized due to oscillatory behavior of superconducting correlations in NF region inside the weak-link area, which connects SN electrodes. So there are infinite number of point curves. The point curves at which I_C=0 looks like practically vertical lines thus demonstrating weak influence of overlap distance d on alternation of 0 and π states in the junction.

Finally, Figs. 8 and 9 give $(L/\xi_N, d/\xi_N)$ phase diagrams for SNF-FN-FNS junctions. In these structures, coherence lengths are complex both under superconductor in complex SNF electrodes and in NF part of weak-link region. The appearance of 0 or π state in this case depends also on matching these oscillations at SNF/NF boundary. As a result, the point curves at which I_C=0 are not as vertical as those one can see in Figs. 6 and 7 thus demonstrating their strong dependence on both lengths L/ξ_N and d, and the 0-π transition with d increase is not so sensitive to L variations as for SN-FN-NS structure.

Figure 10 shows dependence of absolute value of normalized critical currents of SNF-NF-FNS, SNF-N-FNS, SN-NF-NS, and SFNS junctions as a function of L/ξ_N for infinite length of SN interface d. It is seen that at given magnitude of L/ξ_N critical current of SN-N-NS junction, $I_C^{\text{SN-N-NS}}$, has the maximum value among all others. This fact is obvious since in this structure there is no additional suppression of superconductivity provided by the F film. If we compare the value of I_C far from the 0-π transition points for all other considered structures, then we may have $I_C^{\text{SN-FN-NS}} > I_C^{\text{SNF-N-FNS}} > I_C^{\text{SNF-FN-FNS}} > I_C^{\text{S-FN-S}}$. This sequence of values is due to consecutive increase in suppression of superconductivity provided by F film.

In SN-FN-NS junctions in the considered region of parameters the superconducting correlations are suppressed by F film only in weak-link region, thus providing the large value of I_C. In SNF-N-FNS junctions, the critical current is smaller than in SN-FN-NS devices due to suppression of superconductivity in SNF part of the structure. Due to it, the decay of superconducting correlations into N part of weak link starts from the values, which are smaller than in SN-FN-NS devices.

In SNF-FN-FNS devices, there is suppression of superconductivity in all parts of structure by F film. Finally, in SNFS ramp-type structures the critical current has the smallest value. The physical reason of this fact, we already discussed in Sec. III.

In SN-N-NS and SNF-N-FNS junctions, I_C decays with L without oscillations. However, as it follows from the phase

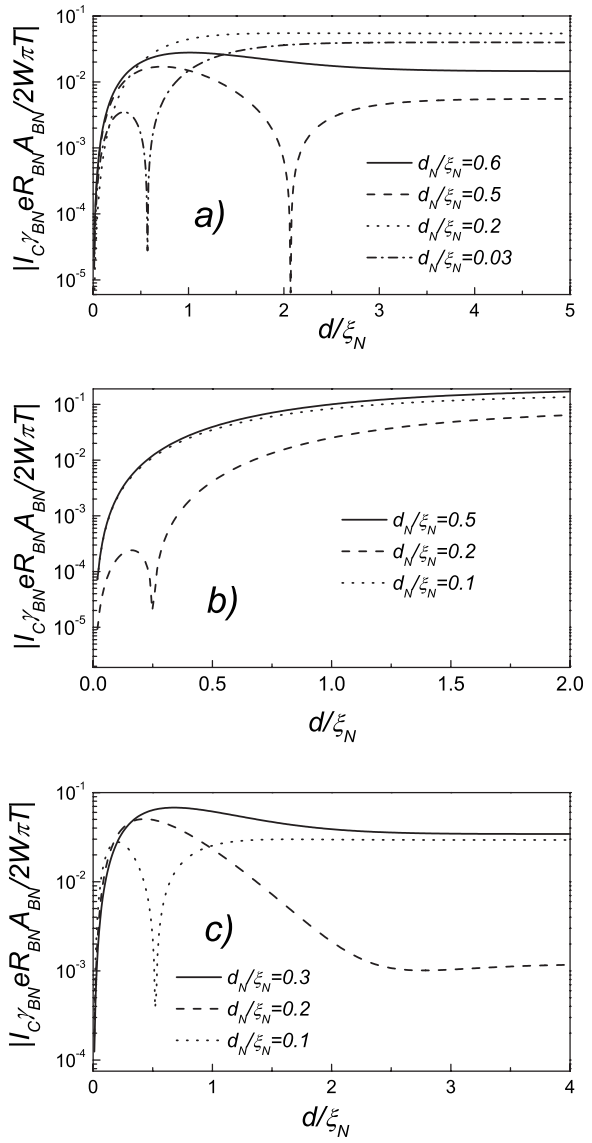

FIG. 11. I_C for (a) SNF-FN-FNS, (b) SN-FN-NS, (c) SNF-N-FNS structures versus d/ξ_N calculated at $\xi_N/\xi_F=10$, $T/T_C=0.5$, $H/\pi T_C=30$, $d_F/\xi_F=0.1$, and $L/\xi_N=2$.

diagram presented in Fig. 4, under the chosen set of parameters the SNF-N-FNS structure is the π state, so that its critical current is negative, while SN-N-NS is always in 0 state.

The decay length in NF part of SN-FN-NS, SNF-FN-FNS, and SNFS devices is complex providing damping oscillations of I_C as a function of L. The period of these oscillations and their decay length are the same for all the junctions and controlled by bulk properties of NF part of weak link. The initial conditions for these oscillations at SN/NF, SNF/FN, and S/NF interfaces are different resulting in shift of the oscillations along L axis.

Figure 11 shows the amplitude of critical current of SNF-FN-FNS, SN-FN-NS, and SNF-N-FNS structures versus the length of SN interface in complex electrodes calculated under fixed ratio of $L/\xi_N=2$. From the presented curves, it follows that critical currents have a tendency to increase with d as $\tanh^2(d/\xi_N)$ while at large d they arrive at is independent of d values.

The continuous support of superconductivity from the S electrodes along all the SN interfaces results in considerable difference between $I_C(L)$ and $I_C(d)$ dependencies. The last may have only one change in sign of I_C as a function of d.

It is also necessary to note that maximum of I_C in $I_C(d)$ dependence may *be not necessarily* achieved in the limit of $d\to\infty$. For instance, at $d_N/\xi_N=0.2$ and $d/\xi_N=0.5$ [see Fig. 11(c)] the magnitude of I_C is 50 times larger compared to the value, which is reached at $d\to\infty$. This strong enhancement may be important for some practical applications of these structures.

V. CONCLUSION

We have discussed *three* types of SFNS Josephson junctions with different geometries of electrodes (S electrodes are on the top of N film) and weak links. We derived analytical expressions for critical currents of these structures. These expressions are valid in the limit of thin normal and ferromagnetic films, and we discussed behavior of critical currents for this case. Hence, we assert that one can use expressions for critical currents with more accurate formula for inverse coherence length, Eq. (25), for films with arbitrary thickness.

We compared results of this paper with results for ramp-type S-FN-S Josephson junctions. The ramp-type junctions are absolutely not favorable both from technological and applicable point of view. We have demonstrated that I_C of SN-NF-NS, SNF-NF-NFS, or SNF-N-NFS junctions can be even large compared to that in the ramp-type structures under the same suppression parameters at NS interface and distance between S electrodes. The largest value of critical current can be achieved in SN-NF-NS junction in which there are no additional suppressions from F film under S electrode.

We have predicted that in these structures 0-π transition takes place not only under increase in the distance L between the superconducting electrodes but also as a result of changing the area of Cooper-pair injection under the S electrodes. As a result, there is single 0-π transition, in contrast to multiple transitions with the increase in the distance L between superconducting electrodes. We also demonstrated that in SNF-N-FNS structures, where coherence length in the weak link is not complex, critical current can change sign as a function of distance L.

From the above-performed analysis of the processes in Josephson variable thickness bridges, in which superconducting electrodes are located on the top of NF bilayer, it follows that their properties may considerably differ from those of SFNS ramp-type structures. In ramp-type devices, the weak-link area is strictly determined by geometrical factors, namely, by the distance L between superconducting electrodes. Under conditions, which minimize suppression of superconductivity in the S electrodes, the initial values of anomalous Green's function at SN and SF interfaces are strictly fixed by boundary conditions and 0-π transition is a result of interplay between the complex value of decay length in the NF bilayer and its geometrical size L.

In the structures shown in Figs. 2(a)–2(c), the area of the weak link may not coincide with the distance L between superconductors since superconductivity induced into NF bilayer is influenced by proximity effect with the part of weak link not covered by superconductor. It means that the boundary conditions at SNF/NF interfaces are soft and do not fix initial conditions for $I_C(L)$ dependence thus providing additional degree of freedom responsible for 0-π transition in the considered structures. This feature is most clearly revealed in SNF-N-FNS junctions. In these devices the decay length in a part of N film located in between of SNF electrodes is a real quantity, which prevents the oscillations of function Φ_N in that region of the N film. However, 0-π transition may take place in these structures despite of the absence of oscillations of function Φ_N in the region between SNF electrodes. It is worth to mention that in the latter case there is possibility for only a single 0-π transition. From practical point of view it means that SNF-N-FNS geometry provides the opportunity to realize a π state keeping simultaneously the large value of the critical current.

The second conclusion of our study is illustrated in Fig. 10. One can see that the absolute values of the critical current of the considered devices exceed those in SNFS ramp-type junctions. This difference comes from the fact that in ramp-type configuration superconducting correlation are induced directly into interelectrode coupling area across the cross section of N and F films. In the considered limit of small SN interface transparency this results in small values of superconducting correlations (on the order of Δ/γ_{BN}) induced into vicinity of S/N interface. Contrary to that, in the overlap geometry [see Figs. 2(a)–2(c)] the superconducting correlations induced into the area located under S electrode can be large enough, on the order of $\Delta/(\gamma_{BN}d_N/\xi_N)$ if d_N is considerably smaller than ξ_N. It is necessary to mention that this increase in magnitude of I_C is supplemented by decrease in normal junction resistance, R_N. In the last part of Appendix D we have calculated R_N and have shown that for large d it scales as $\gamma_{BN}^{1/2}$ providing the values of I_CR_N product proportional to $\gamma_{BN}^{-3/2}$ while in ramp-type devices $I_CR_N \propto \gamma_{BN}^{-1}$ decreases more slowly with γ_{BN}.

ACKNOWLEDGMENTS

This work was supported by RFBR under Project No. 09-02-12176 ofi-m, AvH Project 2C0704 "Nonuniform superconductivity in layered SF-nanostructures Superconductor/Ferromagnet" and by NanoNed under Project No. TCS.7029. We thank H. Hahn, V. V. Bol'ginov, and V. V. Ryazanov for fruitful discussions.

APPENDIX A: CALCULATION OF SUPERCURRENT FOR SNF-NF-FNS JUNCTION

To calculate critical current of SNF-NF-FNS Josephson junction in the framework of formulated in Sec. II model it is enough to solve linearized Usadel equations for condensate functions of normal (Φ_N) and ferromagnetic (Φ_F) films in weak-link region, as well as for condensate functions in N films under left (Φ_{N1}) and right (Φ_{N2}) superconducting electrodes. These equations have the form

$$\xi_N^2\left\{\frac{\partial^2}{\partial x^2}+\frac{\partial^2}{\partial y^2}\right\}\Phi_{N,N1,N2}-\Omega\Phi_{N,N1,N2}=0,$$

$$\xi_F^2\left\{\frac{\partial^2}{\partial x^2}+\frac{\partial^2}{\partial y^2}\right\}\Phi_{F,F1,F2}-\tilde{\Omega}\Phi_{F,F1,F2}=0. \tag{A1}$$

They should be supplemented by the boundary conditions on SN interfaces at $x=d_N$,

$$\gamma_{BN}\xi_N\frac{\partial}{\partial x}\Phi_{N1,N2}=G_0\Delta\ \exp^{\mp i\varphi/2}, \tag{A2}$$

where sign minus (plus) should be chosen for left (right) S electrode. At FN interface located at $x=0$ the boundary conditions have the form,

$$\frac{\xi_N}{\Omega}\frac{\partial}{\partial x}\Phi_{N,N1,N2}=\gamma\frac{\xi_F}{\tilde{\Omega}}\frac{\partial}{\partial x}\Phi_{F,F1,F2}, \tag{A3}$$

$$\gamma_B\xi_F\frac{\partial}{\partial x}\Phi_{F,F1,F2}+\Phi_{F1}=\frac{\tilde{\Omega}}{\Omega}\Phi_{N,N1,N2} \tag{A4}$$

while at free interfaces

$$\frac{\partial}{\partial y}\Phi_{N1,N2}=0,\quad y=\mp(L/2+d),$$

$$\frac{\partial}{\partial y}\Phi_{F1,F2}=0,\quad y=\mp(L/2+d), \tag{A5}$$

$$\frac{\partial}{\partial x}\Phi_{F,F1,F2}=0,\quad x=-d_F, \tag{A6}$$

$$\frac{\partial}{\partial x}\Phi_N=0,\quad x=d_N, \tag{A7}$$

they are followed from the demand of preventing a current flow across them. Finally at the interfaces between complex electrodes and weak-link region (at $y=\mp L/2$) all the functions and their first derivatives should be uninterrupted,

$$\frac{\partial}{\partial y}\Phi_{N1,N2}=\frac{\partial}{\partial y}\Phi_N, \tag{A8}$$

$$\Phi_{N1,N2}=\Phi_N, \tag{A9}$$

$$\frac{\partial}{\partial y}\Phi_{F1,F2}=\frac{\partial}{\partial y}\Phi_F, \tag{A10}$$

$$\Phi_{F1,F2}=\Phi_F. \tag{A11}$$

In the considered limit of thin F and N films,

$$d_N \ll \xi_N,\quad d_F \ll \xi_F,$$

the two-dimensional boundary problem, Eqs. (A1)–(A11), can be reduced to a one dimensional. To do this we can

suppose that in the main approximation condensate functions do not depend on coordinate x,

$$\Phi_{N,N1,N2} = A_{N,N1,N2}(y), \quad \Phi_{F,F1,F2} = B_{F,F1,F2}(y), \tag{A12}$$

and that their derivatives with respect to x can be expressed as follows:

$$\frac{\partial \Phi_{N,N1,N2}}{\partial x} = \left\{ \frac{\Omega}{\xi_N^2} A_{N,N1,N2} - \frac{\partial^2 A_{N,N1,N2}}{\partial y^2} \right\} (x - d_N),$$

$$\frac{\partial \Phi_{F,F1,F2}}{\partial x} = \left\{ \frac{\tilde{\Omega}}{\xi_F^2} B_{F,F1,F2} - \frac{\partial^2 B_{F,F1,F2}}{\partial y^2} \right\} (x + d_F). \tag{A13}$$

After substitution of Eqs. (A12) and (A13) into the boundary conditions (A3) and (A4) we arrive at one-dimensional differential equations with respect to functions $A_{N,N1,N2}(y)$ and $B_{F,F1,F2}(y)$. Solution of thus obtained one-dimensional boundary problem for the weak-link region can be expressed in the form,

$$A_N = A_1 \cosh(q_1 y) + A_2 \sinh(q_1 y) + \frac{\beta}{\zeta_N^2} \frac{\Omega}{\tilde{\Omega}} [B_1 \cosh(q_2 y) + B_2 \sinh(q_2 y)], \tag{A14}$$

$$B_F = B_1 \cosh(q_2 y) + B_2 \sinh(q_2 y) - \frac{\beta}{\zeta_F^2} \frac{\tilde{\Omega}}{\Omega} [A_1 \cosh(q_1 y) + A_2 \sinh(q_1 y)], \tag{A15}$$

where fundamental wave vectors of the problem,

$$q_{1,2}^2 = \frac{1}{2} [u^2 + v^2 \mp \sqrt{(u^2 - v^2)^2 + 4\zeta_F^{-2} \zeta_N^{-2}}], \tag{A16}$$

$$u^2 = \left(\frac{1}{\zeta_N^2} + \frac{\Omega}{\xi_N^2} \right), \quad v^2 = \left(\frac{1}{\zeta_F^2} + \frac{\tilde{\Omega}}{\xi_F^2} \right), \tag{A17}$$

and $\zeta_F^2 = \gamma_B d_F \xi_F$, $\zeta_N^2 = \gamma_B d_N \xi_N / \gamma$, and $\beta = (q_1^2 - v^2)^{-1}$.

The appropriate solutions for F and N films located under S electrodes are

$$A_{N1,N2} = A_{11,12} \cosh(q_1 y) + A_{12,22} \sinh(q_1 y) + \frac{\beta}{\zeta_N^2} \frac{\Omega}{\tilde{\Omega}} [B_{11,12} \cosh(q_2 y) + B_{12,22} \sinh(q_2 y)] - N e^{\mp i\varphi/2}, \tag{A18}$$

$$B_{F1,F2} = B_{11,12} \cosh(q_2 y) + B_{12,22} \sinh(q_2 y) - \frac{\beta}{\zeta_F^2} \frac{\tilde{\Omega}}{\Omega} [A_{11,12} \cosh(q_1 y) + A_{12,22} \sinh(q_1 y)] - F e^{\mp i\varphi/2}. \tag{A19}$$

The integration coefficients in Eqs. (A14), (A15), (A18), and (A19) can be found by substituting these expressions into the boundary conditions. This procedure leads to

$$A_1 = \frac{\cos(\varphi/2)\sinh(q_1 d)}{\sinh[q_1(L/2+d)]} \frac{F\beta\zeta_N^{-2} - N}{\nu + 1},$$

$$A_2 = \frac{i \sin(\varphi/2)\sinh(q_1 d)}{\cosh[q_1(L/2+d)]} \frac{F\beta\zeta_N^{-2} - N}{\nu + 1},$$

$$B_1 = -\frac{\cos(\varphi/2)\sinh(q_2 d)}{\sinh[q_2(L/2+d)]} \frac{N\beta\zeta_F^{-2} + F}{\nu + 1},$$

$$B_2 = -\frac{i \sin(\varphi/2)\sinh(q_2 d)}{\cosh[q_2(L/2+d)]} \frac{N\beta\zeta_F^{-2} + F}{\nu + 1}, \tag{A20}$$

where

$$N = \frac{1}{\xi_N d_N} \frac{2v^2 \zeta_N^2 \zeta_F^2}{1 - 4v^2 u^2 \zeta_N^2 \zeta_F^2} \frac{G_0 \Delta}{\gamma_{BN}},$$

$$F = \frac{\tilde{\Omega}}{\Omega} \frac{1}{\xi_N d_N} \frac{\zeta_N^2}{1 - 4v^2 u^2 \zeta_N^2 \zeta_F^2} \frac{G_0 \Delta}{\gamma_{BN}},$$

and $\nu = \beta^2 \zeta_N^{-2} \zeta_F^{-2}$.

By substituting the solution, Eqs. (A14), (A15), and (A20), into general formula for supercurrent, Eq. (15), we obtain the expression for supercurrent in the SNF-NF-FNS structure,

$$I_S = (I_{C1} + I_{C2}) \sin(\varphi), \tag{A21}$$

where

$$I_{C2} = \frac{K \zeta_F^2 \zeta_N^2}{\xi_N d_N} \mathrm{Re} \sum_{\omega=0}^{\infty} \frac{q_2 \Gamma (1 + v^2\beta)^2 (\nu + 1)^{-1} \sinh(q_2 d)^2}{(1 - v^2 u^2 \zeta_F^2 \zeta_N^2)^2 \sinh[q_2(L + 2d)]},$$

$$I_{C1} = \frac{K}{\xi_N d_N} \mathrm{Re} \sum_{\omega=0}^{\infty} \frac{q_1 \Gamma (v^2 \zeta_F^2 \zeta_N^2 - \beta)^2 (\nu + 1)^{-1} \sinh(q_1 d)^2}{(1 - v^2 u^2 \zeta_F^2 \zeta_N^2)^2 \sinh[q_1(L + 2d)]},$$

and $\Gamma = \Delta^2 / (\Omega^2 + \Delta^2)$.

In the limit, $\zeta_N \gg \zeta_F$, $\xi_N \gg \xi_F$, the part of the full critical current, I_{C2}, is small, so that the magnitude of I_C of SNF-NF-FNS structure is reduced to

$$I_C^{\text{SNF-NF-FNS}} = \frac{K}{\xi_N d_N} \sum_{\omega=0}^{\infty} \mathrm{Re} \frac{\Gamma U q_1 \sinh(q_1 d)^2}{\sinh[q_1(L + 2d)]}.$$

APPENDIX B: CALCULATION OF SUPERCURRENT FOR SNF-N-FNS JUNCTION

To calculate supercurrent across SNF-N-FNS junction we should slightly change the procedure described in Appendix A by taking into account the appearance of additional three interfaces in the structure. Since the current cannot flow across them instead of Eq. (A11) we should use

$$\frac{\partial}{\partial y} \Phi_{F1,F2} = 0, \quad y = \mp L/2, \quad -d_F \le z \le 0, \tag{B1}$$

$$\frac{\partial}{\partial x}\Phi_N = 0, \quad x = 0, \quad -\frac{L}{2} \le y \le \frac{L}{2}. \tag{B2}$$

In the limit of thin F and N films $d_N \ll \xi_N$, $d_F \ll \xi_F$, the solution of Usadel equations in the N film of weak link has more simple form compared to Eq. (A14),

$$A_N = A_1 \cosh(qy) + A_2 \sinh(qy) \tag{B3}$$

while in FN bilayer under S electrodes it is closest to that of Eqs. (A18) and (A19),

$$A_{N1,N2} = A_{11,12}\cosh(q_1 y) + A_{12,22}\sinh(q_1 y) + \frac{\beta}{\zeta_N^2}\frac{\Omega}{\tilde{\Omega}}[B_{11,12}\cosh(q_2 y) + B_{12,22}\sinh(q_2 y)] - Ne^{\mp i\varphi/2}, \tag{B4}$$

$$B_{F1,F2} = B_{11,12}\cosh(q_2 y) + B_{12,22}\sinh(q_2 y) - \frac{\beta}{\zeta_F^2}\frac{\tilde{\Omega}}{\Omega}[A_{11,12}\cosh(q_1 y) + A_{12,22}\sinh(q_1 y)] - Fe^{\mp i\varphi/2}. \tag{B5}$$

The integration constants in Eqs. (B3)–(B5) can be found from the boundary conditions. In particular, for A_1 and A_2 one can get

$$A_1 = \frac{-N\cos\{\varphi/2\}}{(Q_{q_1,q/2} + \nu Q_{q_2,q/2})/(\nu+1)\tanh\dfrac{qL}{2} + \cosh\dfrac{qL}{2}}, \tag{B6}$$

$$A_2 = \frac{-iN\sin\{\varphi/2\}}{(Q_{q_1,q/2} + \nu Q_{q_2,q/2})/(\nu+1) + \sinh\dfrac{qL}{2}}. \tag{B7}$$

Substitution of Eqs. (B3), (B6), and (B7) into general formula for supercurrent,

$$I_S = -\frac{i\pi TW}{e\rho_N}\sum_{n=-\infty}^{\infty}\frac{1}{\omega^2}\int_0^{d_N}\left[\Phi^*_{-\omega,N}\frac{\partial}{\partial y}\Phi_{\omega,N}\right],$$

in the limit $\zeta_N \gg \zeta_F$, $\xi_N \gg \xi_F$ leads to

$$I_C^{\text{SNF-N-FNS}} = \frac{K}{\xi_N d_N}\mathrm{Re}\sum_{n=0}^{\infty}\frac{\Gamma U q}{Q_{q_1,q} + P_{q_1,q}}, \tag{B8}$$

where functions $Q_{q_1,q}$ and $P_{q_1,q}$ are determined by Eqs. (20) and (21), respectively.

APPENDIX C: CALCULATION OF SUPERCURRENT FOR SN-NF-NS JUNCTION

To calculate supercurrent across SN-FN-NS junction we should change the procedure described in Appendix A by taking into account the absence of F film in complex SN electrode. To do this the boundary conditions, Eq. (A11), in appropriate regions should be replaced by

$$\frac{\partial}{\partial y}\Phi_F = 0, \quad y = \mp L/2, \quad -d_F \le x \le 0, \tag{C1}$$

$$\frac{\partial}{\partial x}\Phi_{N1,N2} = 0, \quad x = 0, \quad \frac{L}{2} \le |y| \le \frac{L}{2} + d. \tag{C2}$$

In the limit of thin F and N films $d_N \ll \xi_N$, $d_F \ll \xi_F$, solution of the boundary problem in the weal link can be found in the form,

$$A_N = A_1\cosh(q_1 y) + A_2\sinh(q_1 y) + \frac{\beta}{\zeta_N^2}\frac{\Omega}{\tilde{\Omega}}[B_1\cosh(q_2 y) + B_2\sinh(q_2 y)], \tag{C3}$$

$$B_F = B_1\cosh(q_2 y) + B_2\sinh(q_2 y) - \frac{\beta}{\zeta_F^2}\frac{\tilde{\Omega}}{\Omega}[A_1\cosh(q_1 y) + A_2\sinh(q_1 y)] \tag{C4}$$

while for it, in the N films located under S electrodes, they are

$$A_{N1,N2} = A_{11,12}\cosh(q_1 y) + A_{12,22}\sinh(q_1 y) - Ne^{\mp i\varphi/2}. \tag{C5}$$

Integration constants A_1, A_2, B_1, B_2 in Eqs. (C3)–(C5) can be found from the boundary conditions resulting in

$$A_1 = \frac{\cos(\varphi/2)q^{-2}G_0\Delta/(\xi_N d_N \gamma_{BN})}{\cosh\dfrac{q_1 L}{2} + [\nu Q_{q_2/2,q_1/2}/2 + Q_{q,q_1/2}(\nu+1)]\tanh\dfrac{q_1 L}{2}},$$

$$A_2 = \frac{i\sin\{\varphi/2\}q^{-2}G_0\Delta/(\xi_N d_N \gamma_{BN})}{\sinh\dfrac{q_1 L}{2} + \nu\tanh^2\left(\dfrac{q_2 L}{2}\right)Q_{q_2/2,q_1/2}/2 + Q_{q,q_1/2}(\nu+1)}, \tag{C6}$$

$$B_1 = A_1\frac{1}{\zeta_F^2}\beta\frac{\tilde{\omega}}{|\omega|}\frac{q_1\sinh(q_1 L/2)}{q_2\sinh(q_2 L/2)}, \tag{C7}$$

$$B_2 = A_2\frac{1}{\zeta_F^2}\beta\frac{\tilde{\omega}}{|\omega|}\frac{q_1\cosh(q_1 L/2)}{q_2\cosh(q_2 L/2)}. \tag{C8}$$

Substituting this result into general formula for supercurrent, Eq. (15), in the limit $\zeta_N \gg \zeta_F$, $\xi_N \gg \xi_F$ we arrived at the following formula for critical current of the SN-FN-NS junction:

$$I_C^{\text{SN-NF-NS}} = \frac{K}{\xi_N d_N}\mathrm{Re}\sum_{n=0}^{\infty}\frac{\Gamma q_1}{q^4(Q_{q,q_1} + P_{q,q_1})}.$$

APPENDIX D: CALCULATION OF NORMAL JUNCTION RESISTANCE

To calculate the normal junction resistance, R_N, of SN-NF-NS junction it is enough to solve in F and F films the

Laplace equations for electric potential $U(x,z)$,

$$\frac{\partial^2}{\partial x^2}U(x,y)+\frac{\partial^2}{\partial y^2}U(x,y)=0, \tag{D1}$$

for $y\geq 0$. The following boundary conditions for this equation at $x=d_N$, $0\leq y\leq \frac{L}{2}$, and $x=-d_F$, $0\leq y\leq \frac{L}{2}+d$ follow from the requirement of absence of normal current flow across these interfaces,

$$\frac{\partial}{\partial x}U(x,y)=0. \tag{D2}$$

At $x=d_N$, $\frac{L}{2}\leq y\leq \frac{L}{2}+d$ the local current density in x direction should be equal to the density of the normal current injected into S electrode from N film,

$$\sigma_N\frac{\partial}{\partial x}U(x,y)=\frac{U_0-U(x,y)}{R_{BN}\mathcal{A}_{B1}}, \tag{D3}$$

and at $y=0$, $0\leq x\leq d_N$, and $-d_F\leq x\leq 0$ the first derivative of electric potential should be determined by the full currents I_N and I_F flow across cross sections of N and F films, respectively,

$$\frac{\partial}{\partial y}U(x,y)=\begin{cases}\dfrac{I_N}{\sigma_N W d_N}, & 0\leq x\leq d_N\\ \dfrac{I_F}{\sigma_F W d_F}, & -d_F\leq x\leq 0.\end{cases} \tag{D4}$$

Finally, at FN interface electric potential should satisfy the following matching conditions:

$$U(+0,y)=U(-0,y), \tag{D5}$$

$$\sigma_N\frac{\partial}{\partial z}U(+0,y)=\sigma_F\frac{\partial}{\partial z}U(-0,y). \tag{D6}$$

Here $\sigma_N(\sigma_F)$ are normal conductivities of N (F) films, R_{BN} and $\mathcal{A}_{B1}$ are boundary resistance and area of SN interface, respectively, d_N and d_F are the thickness of N and F films, U_0 is electric potential of S electrode, which is supposed to be independent of x. Physically the boundary condition (D3) means that we neglect (compare to SN interface resistance) the contribution to R_N from a part of S electrode in which the final transformation from normal to supercurrent takes place in S film and suppose that this conversation is fully located at SN interface.

Below we will essentially use the fact that both d_N and d_F are thin in scales of L, d, and λ,

$$d_N,d_F\ll L,d,\lambda, \tag{D7}$$

where λ is specific scale, which is characterized by the process of redistribution of the current occurring in different areas of the structure.

Solution of the boundary problem, Eqs. (D1)–(D6), under condition (D7) at $0\leq y\leq L/2$ has the form,

$$U=\begin{cases}Q_1 y+A_1\cos\dfrac{x-d_N}{\lambda}\cosh\dfrac{y}{\lambda}, & 0\leq x\leq d_N\\ Q_2 y+A_2\cos\dfrac{x+d_F}{\lambda}\cosh\dfrac{y}{\lambda}, & -d_F\leq x\leq 0.\end{cases} \tag{D8}$$

In the region $L\leq y\leq L+d$ we also have

$$U=U_0+A_3\cos\frac{x-d_N}{\lambda}\cosh\frac{x-L/2-d}{\lambda}+B_3\sin\frac{x-d_N}{\lambda}\cosh\frac{y-L/2-d}{\lambda},$$

for $0\leq x\leq d_N$, and

$$U(x,y)=U_0+A_4\cos\frac{x+d_F}{\lambda}\cosh\frac{y-L/2-d}{\lambda}, \tag{D9}$$

for $-d_F\leq x\leq 0$. On matching Eqs. (D5) and (D6) and boundary, Eq. (D3), conditions to solutions (D8) and (D9) and taking into account that all of them must be satisfied identically for any y we arrived at

$$Q_1=Q_2,\quad A_1=0,\quad A_2=0, \tag{D10}$$

$$A_3=A_4=-\frac{\lambda\sigma_N}{\sigma_N d_N+\sigma_F d_F}B_3, \tag{D11}$$

$$\lambda^2=R_{BN}\mathcal{A}_{B1}(\sigma_N d_N+\sigma_F d_F). \tag{D12}$$

To relate the potential U_0 with the full current $I=I_N+I_F$ across the junction we may simply use Eq. (D4) and from Eq. (D10) get,

$$Q_1=\frac{I}{W(\sigma_N d_N+\sigma_F d_F)}. \tag{D13}$$

Calculating now the magnitude of electric potential at $y=L/2$,

$$\frac{I}{W(\sigma_N d_N+\sigma_F d_F)}L=U_0-\frac{\lambda\sigma_N}{\sigma_N d_N+\sigma_F d_F}B_3\cosh\frac{d}{\lambda}$$

and taking into account the condition of current continuity at $x=L$,

$$\frac{I}{W(\sigma_N d_N+\sigma_F d_F)}=\frac{\sigma_N}{\sigma_N d_N+\sigma_F d_F}B_3\sinh\frac{d}{\lambda},$$

for the normal junction resistance, R_N, we finally get

$$R_N=\frac{L}{W(\sigma_N d_N+\sigma_F d_F)}\left(1+\frac{\lambda}{L}\coth\frac{d}{\lambda}\right), \tag{D14}$$

$$\lambda=\sqrt{R_{BN}\mathcal{A}_{B1}(\sigma_N d_N+\sigma_F d_F)}. \tag{D15}$$

In the limit $d_F\to 0$ expression (D14) transforms to that previously derived in Ref. 62.

Application of the developed method of R_N calculation to SNF-N-FNS and SN-NF-NS structures leads to

$$R_N = \frac{L}{W\sigma_N d_N}\left(1 + \frac{\lambda}{L}\coth\frac{d}{\lambda}\right), \tag{D16}$$

$$\lambda = \sqrt{R_{BN}\mathcal{A}_{B1}(\sigma_N d_N + \sigma_F d_F)} \tag{D17}$$

and

$$R_N = \frac{L}{W(\sigma_N d_N + \sigma_F d_F)}\left(1 + \frac{\lambda}{L}\coth\frac{d}{\lambda}\right), \tag{D18}$$

$$\lambda = \sqrt{R_{BN}\mathcal{A}_{B1}\sigma_N d_N}, \tag{D19}$$

respectively.

[1] A. A. Golubov, M. Yu. Kupriyanov, and E. Il'ichev, Rev. Mod. Phys. **76**, 411 (2004).
[2] F. S. Bergeret, A. F. Volkov, and K. B. Efetov, Rev. Mod. Phys. **77**, 1321 (2005).
[3] A. I. Buzdin, Rev. Mod. Phys. **77**, 935 (2005).
[4] L. B. Ioffe, V. B. Geshkenbein, M. V. Feigel'man, A. L. Fauchère, and G. Blatter, Nature (London) **398**, 679 (1999).
[5] A. V. Ustinov and V. K. Kaplunenko, J. Appl. Phys. **94**, 5405 (2003).
[6] G. Blatter, V. B. Geshkenbein, and L. B. Ioffe, Phys. Rev. B **63**, 174511 (2001).
[7] E. Terzioglu and M. R. Beasley, IEEE Trans. Appl. Supercond. **8**, 48 (1998).
[8] Hans Hilgenkamp, Supercond. Sci. Technol. **21**, 034011 (2008).
[9] V. V. Ryazanov, V. A. Oboznov, A. Y. Rusanov, A. V. Veretennikov, A. A. Golubov, and J. Aarts, Phys. Rev. Lett. **86**, 2427 (2001).
[10] T. Kontos, M. Aprili, J. Lesueur, F. Genet, B. Stephanidis, and R. Boursier, Phys. Rev. Lett. **89**, 137007 (2002).
[11] A. S. Sidorenko, V. I. Zdravkov, J. Kehrle, R. Morari, G. Obermeier, S. Gsell, M. Schreck, C. Muller, M. Yu. Kupriyanov, V. V. Ryazanov, S. Horn, L. R. Tagirov, and R. Tidecks, Pis'ma Zh. Eksp. Teor. Fiz. **90**, 149 (2009) [JETP Lett. **90**, 139 (2009)].
[12] T. Khaire, M. Khasawneh, W. Pratt, Jr., and N. Birge, arXiv:0912.0205 (unpublished).
[13] G. Nowak, H. Zabel, K. Westerholt, I. Garifullin, M. Marcellini, A. Liebig, and B. Hjörvarsson, Phys. Rev. B **78**, 134520 (2008).
[14] P. S. Luo, T. Crozes, B. Gilles, S. Rajauria, B. Pannetier, and H. Courtois, Phys. Rev. B **79**, 140508(R) (2009).
[15] J. Pfeiffer, M. Kemmler, D. Koelle, R. Kleiner, E. Goldobin, M. Weides, A. K. Feofanov, J. Lisenfeld, and A. V. Ustinov, Phys. Rev. B **77**, 214506 (2008).
[16] C. Gürlich, S. Scharinger, M. Weides, H. Kohlstedt, R. Mints, E. Goldobin, D. Koelle, and R. Kleiner, Phys. Rev. B **81**, 094502 (2010).
[17] F. S. Bergeret, A. F. Volkov, and K. B. Efetov, Phys. Rev. Lett. **86**, 4096 (2001).
[18] A. Kadigrobov, R. I. Shekhter, and M. Jonson, Europhys. Lett. **54**, 394 (2001).
[19] F. S. Bergeret, A. F. Volkov, and K. B. Efetov, Phys. Rev. B **64**, 134506 (2001).
[20] A. F. Volkov, F. S. Bergeret, and K. B. Efetov, Phys. Rev. Lett. **90**, 117006 (2003).
[21] F. S. Bergeret, A. F. Volkov, and K. B. Efetov, Phys. Rev. B **68**, 064513 (2003).
[22] Z. Pajović, M. Božović, Z. Radović, J. Cayssol, and A. Buzdin, Phys. Rev. B **74**, 184509 (2006).
[23] B. Crouzy, S. Tollis, and D. A. Ivanov, Phys. Rev. B **75**, 054503 (2007).
[24] I. B. Sperstad, J. Linder, and A. Sudbo, Phys. Rev. B **78**, 104509 (2008).
[25] Y. Tanaka and A. A. Golubov, Phys. Rev. Lett. **98**, 037003 (2007); Y. Asano, Y. Sawa, Y. Tanaka, and A. A. Golubov, Phys. Rev. B **76**, 224525 (2007).
[26] M. Eschrig, J. Kopu, J. C. Cuevas, and G. Schon, Phys. Rev. Lett. **90**, 137003 (2003); M. Eschrig and T. Lofwander, Nat. Phys. **4**, 138 (2008).
[27] V. Braude and Y. V. Nazarov, Phys. Rev. Lett. **98**, 077003 (2007).
[28] M. Houzet and A. I. Buzdin, Phys. Rev. B **76**, 060504(R) (2007).
[29] A. F. Volkov, A. Anishchanka, and K. B. Efetov, Phys. Rev. B **73**, 104412 (2006).
[30] A. F. Volkov, Ya. V. Fominov, and K. B. Efetov, Phys. Rev. B **72**, 184504 (2005)
[31] T. Löfwander, T. Champel, and M. Eschrig, Phys. Rev. B **75**, 014512 (2007).
[32] T. Champel, T. Lofwander, and M. Eschrig, Phys. Rev. Lett. **100**, 077003 (2008).
[33] A. V. Galaktionov, M. S. Kalenkov, and A. D. Zaikin, Phys. Rev. B **77**, 094520 (2008).
[34] F. S. Bergeret, A. F. Volkov, and K. B. Efetov, Appl. Phys. A: Mater. Sci. Process. **89**, 599 (2007).
[35] K. B. Efetov, I. A. Garifullin, A. F. Volkov, and K. Westerholt, *Magnetic Heterostructures*, edited by H. Zabel and S. Bader, Springer Tracts In Modern Physics Vol. 227 (Springer, Berlin, 2008), p. 251.
[36] N. M. Chtchelkatchev and I. S. Burmistrov, Phys. Rev. B **68**, 140501(R) (2003).
[37] Ya. V. Fominov, A. A. Golubov, and M. Yu. Kupriyanov, Pis'ma Zh. Eksp. Teor. Fiz. **77**, 609 (2003) [JETP Lett. **77**, 510 (2003)].
[38] I. S. Burmistrov and N. M. Chtchelkatchev, Phys. Rev. B **72**, 144520 (2005).
[39] T. Champel and M. Eschrig, Phys. Rev. B **72**, 054523 (2005).
[40] M. Houzet and A. I. Buzdin, Phys. Rev. B **74**, 214507 (2006).
[41] M. A. Maleki and M. Zareyan, Phys. Rev. B **74**, 144512 (2006).
[42] Ya. V. Fominov, A. F. Volkov, and K. B. Efetov, Phys. Rev. B **75**, 104509 (2007).
[43] A. F. Volkov and A. Anishchanka, Phys. Rev. B **71**, 024501 (2005).
[44] A. F. Volkov and K. B. Efetov, Phys. Rev. B **78**, 024519 (2008).
[45] B. Crouzy, S. Tollis, and D. A. Ivanov, Phys. Rev. B **76**, 134502 (2007).
[46] F. S. Bergeret, A. F. Volkov, and K. B. Efetov, Phys. Rev. Lett. **86**, 3140 (2001).
[47] E. Koshina and V. Krivoruchko, Phys. Rev. B **63**, 224515 (2001); V. N. Krivoruchko and E. A. Koshina, *ibid.* **64**, 172511 (2001).

[48] A. A. Golubov, M. Yu. Kupriyanov, and Ya. V. Fominov, Pis'ma Zh. Eksp. Teor. Fiz. **75**, 223 (2002) [JETP Lett. **75**, 190 (2002)].
[49] Y. M. Blanter and F. W. J. Hekking, Phys. Rev. B **69**, 024525 (2004).
[50] T. Yu. Karminskaya and M. Yu. Kupriyanov, Pis'ma Zh. Eksp. Teor. Fiz. **85**, 343 (2007) [JETP Lett. **85**, 286 (2007)].
[51] T. Yu. Karminskaya and M. Yu. Kupriyanov, Pis'ma Zh. Eksp. Teor. Fiz. **86**, 65 (2007) [JETP Lett. **86**, 61 (2007)].
[52] T. Yu. Karminskaya, M. Yu. Kupriyanov, and A. A. Golubov, Pis'ma Zh. Eksp. Teor. Fiz. **87**, 657 (2008) [JETP Lett. **87**, 570 (2008)].
[53] T. Yu. Karminskaya, A. A. Golubov, M. Yu. Kupriyanov, and A. S. Sidorenko, Phys. Rev. B **79**, 214509 (2009).
[54] N. G. Pugach, M. Yu. Kupriyanov, A. V. Vedyayev, C. Lacroix, E. Goldobin, D. Koelle, R. Kleiner, and A. S. Sidorenko, Phys. Rev. B **80**, 134516 (2009).
[55] Ya. V. Fominov, A. A. Golubov, T. Yu. Karminskaya, M. Yu. Kupriyanov, R. G. Deminov, and L. R. Tagirov, Pis'ma Zh. Eksp. Teor. Fiz. **91**, 329 (2010).
[56] F. Born, M. Siegel, E. K. Hollmann, H. Braak, A. A. Golubov, D. Y. Gusakova, and M. Yu. Kupriyanov, Phys. Rev. B **74**, 140501(R) (2006).
[57] J. W. A. Robinson, S. Piano, G. Burnell, C. Bell, and M. G. Blamire, Phys. Rev. Lett. **97**, 177003 (2006).
[58] K. K. Likharev, Rev. Mod. Phys. **51**, 101 (1979).
[59] A. A. Golubov, M. Yu. Kupriyanov, and V. F. Lukichev, Mikroelektronika **12**, 342 (1983) [Sov.-Phys. Microelectronics **12**, 180 (1983)].
[60] L. Usadel, Phys. Rev. Lett. **25**, 507 (1970).
[61] M. Yu. Kuprianov and V. F. Lukichev, Zh. Eksp. Teor. Fiz. **94**, 139 (1988) [Sov. Phys. JETP **67**, 1163 (1988)].
[62] M. Yu. Kuprianov, Sverhprovodimost: Fiz., Khim., Tekh. **2**, 5 (1989).